

Synthesis of Three-Dimensional Mesostructured Graphitic Carbon Nitride Materials and their Application as Heterogeneous Catalysts for Knoevenagel Condensation Reactions

Jie Xu · Kang Shen · Bing Xue ·
Yong-Xin Li · Yong Cao

Received: 22 November 2012 / Accepted: 14 March 2013 / Published online: 23 March 2013
© Springer Science+Business Media New York 2013

Abstract Three-dimensional (3D) mesostructured graphitic carbon nitride materials with tunable surface areas ($394\text{--}498\text{ m}^2\text{ g}^{-1}$) and pore volumes ($0.54\text{--}1.36\text{ cm}^3\text{ g}^{-1}$) were synthesized through a nanocasting method. Mesocellular silica foam (MCF) was used as a template, and carbon tetrachloride (CTC) and ethylenediamine (EDA) were used as precursors. The effect of the ratio of the two precursors (EDA/CTC) on the textural properties and chemical compositions of the CN-MCF samples were investigated by several characterization techniques. The results revealed that the 3D mesostructures were maintained when the ratio of EDA/CTC was greater than 0.4. Among the different CN-MCF materials prepared, CN-MCF-0.4 demonstrated the highest catalytic performance for Knoevenagel condensation reactions, mainly because of its high amount of surface N, high surface area, and large pore volume. In addition, the CN-MCF-0.4 catalyst showed good stability as well as versatility for various substrates.

Keywords Carbon nitride · Mesocellular silica foam (MCF) · Knoevenagel condensation · Base catalyst

1 Introduction

Because of its high performance in mechanics, conductivity, field emission, and energy storage [1–3], carbon nitride (CN) material has recently emerged as a promising candidate to complement conventional carbon materials in a wide range of applications [4, 5]. Among the several allotropes of CN [1, 2], graphitic CN (g-CN) with layered structures has been found to be the most stable under ambient conditions [6, 7]. More importantly, because of its unique physicochemical properties, such as semiconductivity, special optical features, energy-storage capacity, and gas-adsorption capacity [8, 9], g-CN has been applied extensively in many fields, including fuel cells [10, 11], photocatalysis [12, 13], gas storage [8, 9], and catalysis [14–18].

The precursors commonly used to synthesize g-CN can be divided into two groups. The first group includes cyanamide [7, 19], dicyanamide [20], and melamine [21–23]. The C/N molar ratios of the final products are close to the theoretical ratio of g-C₃N₄ [24]. As suggested by Kroke et al. [1], the tectonic units of these g-C₃N₄ materials are tri-*s*-triazine or *s*-triazine rings linked by N bridges. The second group of the precursors includes carbon tetrachloride (CTC) and ethylenediamine (EDA) [3, 9, 25, 26]. In spite of its high C content (the molar ratios of C/N are ca. 3–5), the g-CN materials obtained are mainly composed of N-substituted graphitic rings and/or cross-linking of graphitic C–N planes [3]. These rich N-containing groups in the forms of amine and/or imine make g-CN basic, thus enabling it to be a type of metal-free base catalyst [18].

Electronic supplementary material The online version of this article (doi:10.1007/s10562-013-0994-6) contains supplementary material, which is available to authorized users.

J. Xu (✉) · K. Shen · B. Xue · Y.-X. Li (✉)
Jiangsu Key Laboratory of Advanced Catalytic Materials and Technology, College of Chemistry and Chemical Engineering, Changzhou University, Gehu Road 1, Changzhou 213164, Jiangsu, People's Republic of China
e-mail: shine6832@163.com

Y.-X. Li
e-mail: liyxluck@126.com

Y. Cao
Department of Chemistry, Shanghai Key Laboratory of Molecular Catalysis and Innovative Materials, Fudan University, Shanghai 200433, People's Republic of China

Compared with bulk g-CN, mesostructured g-CN materials with large surface areas and nanosized pores promise a potential upgradation in their catalysis and other applications [18]. Therefore, there has been much effort devoted to designing and fabricating mesostructured g-CN materials. Vinu et al. have reported synthesis of two-dimensional (2D) and three-dimensional (3D) mesoporous g-CN materials (MCN-1, MCN-2 and MCN-3) using CTC and EDA as precursors and SBA-15 [2, 25], SBA-16 [27], and IBN-4 [18] as exotemplates. Recently, using mesocellular silica foam (MCF) material as a template [9], Zhao et al. successfully obtained 3D mesostructured g-CN spheres. Unfortunately, these studies focused mainly on the design and development of mesostructured structures, while the application of these g-CN materials in base-catalyzed reactions is still in its infancy [6]. In addition, there are few reports on the effects of textural properties and N content of mesostructured g-CN materials on their catalytic performance.

Knoevenagel condensation reaction is one of the most important C–C forming reactions. It is widely used for the manufacture of valuable α,β -unsaturated carbonyl compounds for perfumes and the pharmaceutical industry [28–30]. Conventionally, Knoevenagel condensation reactions proceed homogeneously in the presence of base catalysts [22], such as ammonia, primary amine, secondary amine, or amino acid. Although these homogeneous catalysts have high catalytic activity, it is difficult to separate and recover the catalysts [28, 31]. Therefore, it is highly required to develop an effectively heterogeneous catalyst for Knoevenagel condensation reaction.

Herein, we report the preparation of 3D mesostructured g-CN materials with tunable surface areas, pore volumes and N content, by using CTC and EDA as precursors and MCF as a template. To demonstrate their catalytic applications, the CN-MCF materials were tested in Knoevenagel condensation reaction. The results show that CN-MCF materials could effectively catalyze the condensation reactions between various aldehydes and methylene-group-containing compounds. These findings provide insight into the design and development of multifunctional 3D g-CN materials as heterogeneous catalysts for wider base-catalyzed organocatalysis processes.

2 Experimental

2.1 Preparation of MCF Material

The MCF material was synthesized using a Pluronic P123 (EO₂₀PO₇₀EO₂₀, M_{av} = 5800, Sigma-Aldrich) triblock copolymer surfactant, and 1,3,5-trimethylbenzene (TMB) as an organic swelling agent [32, 33]. In a typical preparation process, 4 g of P123 was dissolved into 150 mL of

1.6 mol L⁻¹ HCl solution at room temperature. After that, 4.0 g of TMB and 0.046 g of NH₄F were added into the solution, followed by an increase of the reaction temperature to 40 °C for 1 h under vigorous stirring. Next, 8.8 g of tetraethyl orthosilicate was added, and the mixture was further stirred at 40 °C for 20 h. Afterwards, the obtained milky solution was transferred into an autoclave and heated in an oven at 130 °C for 24 h. The white precipitate was filtered off and dried overnight at 60 °C, and then calcined at 550 °C for 5 h to remove the surfactant. Finally, the MCF material was obtained with a mass of ca. 2.3 g.

2.2 Preparation of Mesostructured g-CN Materials

The mesostructured g-CN samples were prepared according to an established nanocasting method [25, 27]. Briefly, 1.0 g of MCF powder was added into a well-mixed solution containing 6.0 g of CTC and 3.6 g of EDA. The mixture was then heated under refluxing at 90 °C for 6 h to induce polymerization of the precursors, and was then dried at 50 °C overnight. Next, the obtained dark-brown solid was heated, starting from room temperature to 600 °C at a ramp of 3 °C min⁻¹. The temperature was kept at 600 °C for another 5 h under an argon atmosphere (30 mL min⁻¹). Afterwards, the sample was washed with NH₄HF₂ aqueous solution (4 mol L⁻¹, 100 mL) to remove the template. The obtained black solid was then centrifuged and washed with distilled water (three times) and ethanol (two times). Finally, the samples were dried at 50 °C under vacuum overnight. The resultant mesostructured g-CN sample was labeled as CN-MCF-*r*, where *r* indicated the weight ratio of EDA to CTC (the mass of CTC was fixed as 6.0 g). For comparison, a bulk g-CN sample (CN-bulk) was also prepared by the same procedure, only without the introduction of MCF material or the post detemplation process.

2.3 Sample Characterization

X-ray diffraction (XRD) patterns of the CN-MCF and CN-bulk samples were recorded with a Bruker D8 Advance X-ray diffractometer equipped with a graphite monochromator, operated at 40 kV and 40 mA, and using Ni-filtered Cu- K_{α} radiation (λ = 1.5418 Å). Small angle X-ray scattering (SAXS) measurements were performed on a Bruker NanoSTAR U SAXS system equipped with a high-resolution pinhole chamber using Cu- K_{α} radiation (40 kV, 35 mA). Nitrogen adsorption–desorption isotherms were measured at –196 °C using a Micromeritics ASAP 2020 analyzer. Prior to the analysis, the samples were degassed (1.33×10^{-2} Pa) at 150 °C for at least 4 h. The specific surface areas were calculated according to the Brunauer-Emmet-Teller (BET) method using adsorption data at relative pressure (p/p°) in the range of 0.05–0.30. The pore

size distribution was determined by the Barret-Joyner-Halenda method. Transmission electron microscopy (TEM) experiments were conducted on a JEOL 2010 electron microscope operating at 200 kV. Before being transferred into the TEM chamber, the samples dispersed in ethanol were deposited onto holey carbon films supported on Cu grids. Fourier transform infrared (FT-IR) spectra of the samples were collected in transmission mode from KBr pellets at room temperature on a Bruker Tensor 27 spectrometer with a resolution of 4 cm^{-1} , using 32 scans per spectrum in the region of $400\text{--}4,000\text{ cm}^{-1}$. The mass ratio of every sample to KBr was constant at 1:200. Raman spectra were recorded on a Raman spectrometer (Jobin-Yvon Lab Ram Infinity) using 514.5 nm line of Ar^+ as an excitation source. X-ray photoelectron spectroscopy (XPS) measurements were performed using a Perkin-Elmer PHI 5000C spectrometer working in the constant analyzer energy mode with $\text{Mg } K_{\alpha}$ radiation as the excitation source. The carbonaceous $\text{C } 1s$ line (284.6 eV) was used as the reference to calibrate the binding energies.

2.4 Catalytic Test

Catalytic tests for Knoevenagel condensation reaction were carried out in a two-neck round bottomed flask (25 mL). 5 mmol of aldehyde, 5 mmol of methylene group-containing nitrile, 0.3 mL of *n*-decane as an internal standard, and 5 mL of solvent (CH_3CN or *n*-butanol as desired) were mixed well. 100 mg of catalyst was added into the mixture and the catalytic tests were performed at $90\text{ }^{\circ}\text{C}$ for 4 h. After the reaction, the mixture was centrifuged and analyzed by GC-MS. The filtered catalyst was washed with ethanol twice, dried overnight, and then investigated for its next running.

3 Results and Discussions

3.1 Catalyst Characterization

XRD patterns of the CN-MCF and CN-bulk samples are shown in Fig. 1. All samples exhibit a single broad diffraction peak near $2\theta = 26^{\circ}$, which is attributed to the (002) plane, characteristic interplanar stacking structures of graphitic materials [2, 3]. A comparison of the diffraction peaks revealed that the *d* spacing (3.46 \AA) calculated from the (002) planes of the CN-MCF samples was slightly higher than that for the bulk one (3.37 \AA). This could arise from defect sites or a curvature of graphitic sheets [34] after the introduction of mesopores into the bulk material. Moreover, for the CN-MCF samples, the intensities of the (002) peak clearly increased with the amount of EDA, showing that g-CN prepared with less EDA has a low

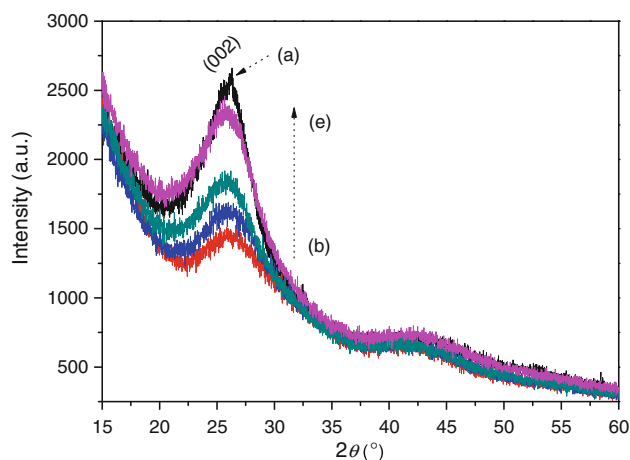


Fig. 1 XRD patterns of CN-bulk and CN-MCF-*r* (*b–e*: *r* = 0.2, 0.4, 0.6, and 0.8) samples

degree of crystallinity. During the synthesis of g-CN materials using CTC and EDA as precursors, the reaction undergoes the condensation polymerization in which N-substituted graphitic rings form with the loss of HCl molecules [2, 3]. In this case, less EDA will induce insufficient condensation of C precursors, and inhibit the growth of rich cross-linking of the graphitic C–N planes.

Figure 2 shows the SAXS patterns of the parent MCF material and resulting CN-MCF samples. Five obvious scattering peaks with exponentially decreasing intensities confirm a well-resolved cellular foam mesostructures for the MCF template [9, 35]. For the CN-MCF-0.4, -0.6, and -0.8 samples, two resolved scattering peaks can be identified, indicating these g-CN samples have the same 3D mesostructures as the template. It is also worth noting that the peaks of the three samples shifted to higher *q* values and the corresponding intensity became weak, which

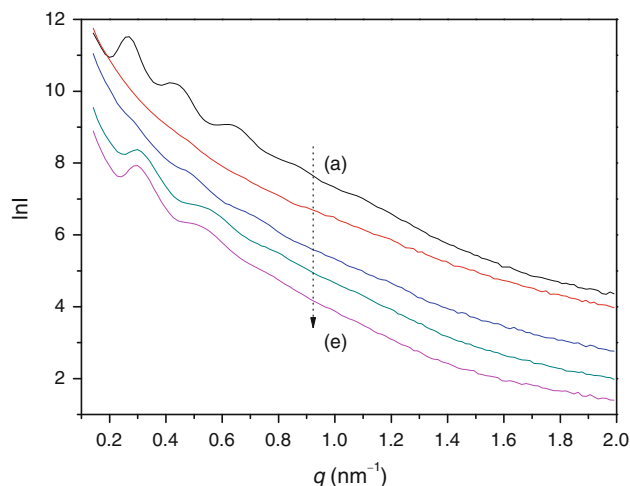


Fig. 2 SAXS patterns of MCF (a) and CN-MCF-*r* (*b–e*: *r* = 0.2, 0.4, 0.6, and 0.8) samples

implies that minor shrinkage occurred in the mesostructures. Few scattering peaks were detected for CN-MCF-0.2, indicating that the original 3D mesostructures of the template have not been retained under the lower amount of EDA. As proposed by Vinu [2] besides acting as N precursor, EDA can reduce the density of the reactant mixture during the preparation of g-CN. At this point, employing higher ratios of EDA/CTC would facilitate the diffusion and filling of the reactant mixture into the 3D porous matrix of the MCF. Consequently, well-defined foamy mesostructures can be maintained after the removal of the template.

The porous nature of MCF and CN-MCF samples was further investigated by N_2 adsorption–desorption (Fig. 3a). MCF displays type IV curves with a steep H1 hysteresis loop at $p/p^\circ = 0.85–0.95$, indicating that the parent material possesses a typical mesoporous structure with large pore size and narrow pore size distribution (PSD) [33].

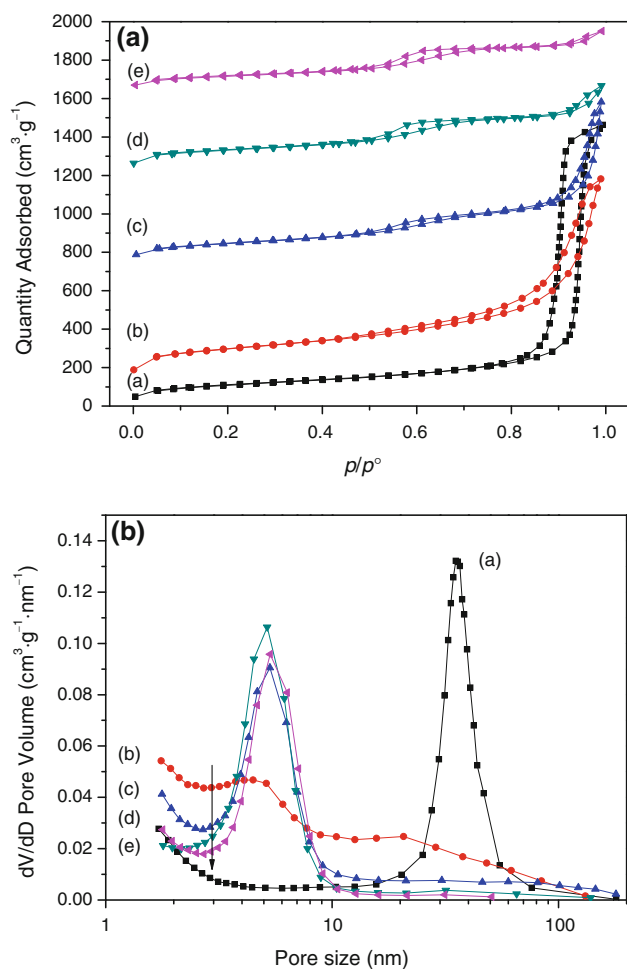


Fig. 3 N_2 adsorption–desorption isotherms (a) and pore size distributions (b) of MCF (a), and CN-MCF- r samples (b–e: $r = 0.2, 0.4, 0.6,$ and 0.8). The isotherms of CN-MCF- r (b–e: $r = 0.2, 0.4, 0.6,$ and 0.8) are shifted by 100, 700, 1200, and 1600, respectively

This result is consistent with the corresponding SAXS pattern. As listed in Table 1, the surface area and total pore volume of MCF reach $391 \text{ m}^2 \text{ g}^{-1}$ and $2.26 \text{ cm}^3 \text{ g}^{-1}$, respectively. Like MCF, all CN-MCF materials present type IV curves with H1 hysteresis loops. This indicates the presence of mesoporous structures for the g-CN samples. Despite this, the CN-MCF samples prepared with various amount of EDA show appreciable differences in terms of their mesostructures. CN-MCF-0.2 exhibited a broad hysteresis loop located at p/p° of $0.60–0.99$, while the three other CN-MCF samples demonstrated two hysteresis loops at p/p° of $0.45–0.65$ and $0.85–0.99$. These results suggest that CN-MCF materials prepared with high amounts of EDA contain characteristic hierarchical mesostructures, namely bimodal mesopores. Accordingly, the PSD curves for the CN-MCF-0.4, -0.6, and -0.8 samples show two peaks, one narrow peak centered at 5 nm (Fig. 3b and Table 1) and the other weak one at 40 nm. In sharp contrast, CN-MCF-0.2 offers very broad peaks at ca. 4 and 11 nm.

Compared with CN-bulk with a low surface area ($<1 \text{ m}^2 \text{ g}^{-1}$) and poor pore volume ($0.03 \text{ cm}^3 \text{ g}^{-1}$), the CN-MCF samples possess appreciably higher surface areas and larger pore volumes (Table 1). This shows that the introduction of the template created porous structures. Furthermore, the influence of the amount of EDA on the BET surface areas and pore volumes of CN-MCF samples can also be shown. The surface area of CN-MCF-0.2 ($675 \text{ m}^2 \text{ g}^{-1}$, Table 1) was much higher than that of its template. Interestingly, as the amount of EDA increased, the surface areas and pore volumes decreased progressively. That is, by adjusting the ratio of EDA/CTC, a series of g-CN materials with tunable surface areas and pore volumes can be created. As mentioned above, less EDA would not only lead to insufficient condensation polymerization but also retard the diffusion of the reactants into the pores of the template. In view of these facts, the extremely

Table 1 Textural properties and chemical compositions of MCF and CN-MCF samples

Sample	S_{BET} ($\text{m}^2 \text{ g}^{-1}$)	Pore size ^a (nm)	V_p^b ($\text{cm}^3 \text{ g}^{-1}$)	Surface N/C ratio ^c
MCF	391	35.7	2.26	–
CN-MCF-0.2	675	4.4	1.67	0.102
CN-MCF-0.4	498	5.3	1.36	0.128
CN-MCF-0.6	446	5.2	0.72	0.101
CN-MCF-0.8	394	5.3	0.54	0.109
CN-bulk	<1	–	<0.03	0.103

^a Determined by the adsorption branch of isotherms

^b Pore volume

^c Calculated by XPS profiles

high surface areas and pore volumes, along with wide PSDs may result from the partial collapse of the g-CN mesostructures [9] and intraparticle voids. Therefore, to fabricate well-replicated mesostructures of CN-MCF materials, the optimal weight ratio of EDA/CTC should be higher than 0.4.

A TEM image (Fig. 4a) of the MCF template reveals a disordered array of silica struts composed of uniform-sized spherical cells (30–40 nm) that are interconnected by windows with a narrow size distribution, which is the characteristic feature of MCF materials [32, 36]. By contrast, the CN-MCF samples show foam-like morphology, suggesting replication of the parent mesostructures. Nevertheless, slight differences can be detected. For CN-MCF-0.2 (Fig. 4b), some macropores (>50 nm) were observed and the PSD was irregular, reflecting some parts of the template remained unfilled during the polymerization of precursors. CN-MCF-0.4 (Fig. 4c) and CN-MCF-0.6 (Fig. 4d) show hexagonal particles with slit pores (ca. 5 nm) between them. This indicates that the original

mesostructures have been replicated, which is in agreement with the results obtained by N₂ adsorption–desorption.

The chemical bonding states of the CN-bulk and CN-MCF samples were characterized by FT-IR spectroscopy (Fig. 5). For CN-bulk, only two weak bands were observed, whereas three pronounced bands at ca. 1,290, 1,610, and 3,455 cm⁻¹ could be identified for all CN-MCF samples. The 1,290 and 1,610 cm⁻¹ bands were assigned to the aromatic C–N stretching bands and aromatic ring modes [37], respectively, while the highest band may represent of the stretching modes of N–H bonds in aromatic rings and –OH stretching vibration of residual water molecules [38]. By further analysis of the intensity of the three bands, it was observed that the intensity of the highest band became gradually weak from CN-MCF-0.2 to CN-MCF-0.8. These profiles may be associated with textural properties of the CN-MCF samples, since more water molecules would be adsorbed by the materials with high surfaces and rich mesostructured pores, resulting in strengthening the intensity of the bands at 3,455 cm⁻¹.

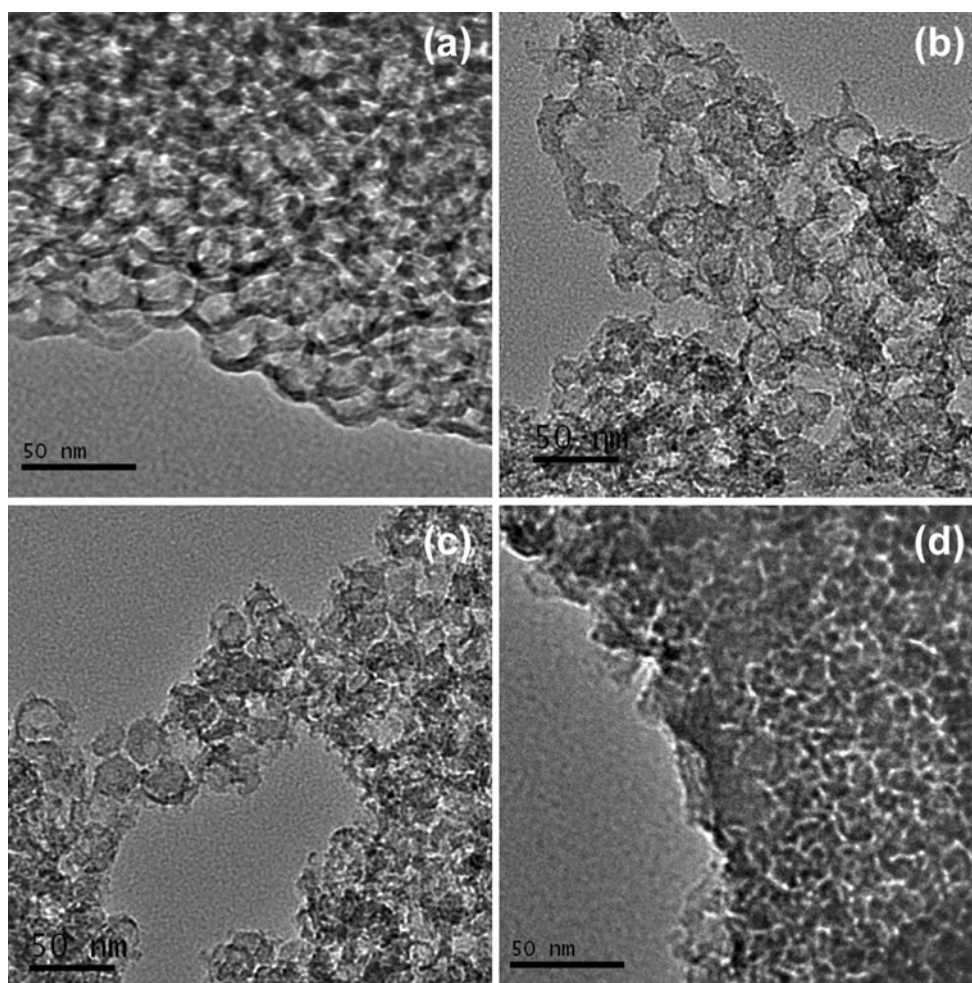


Fig. 4 TEM images of MCF (a), CN-MCF-0.2 (b), CN-MCF-0.4 (c), and CN-MCF-0.6 (d)

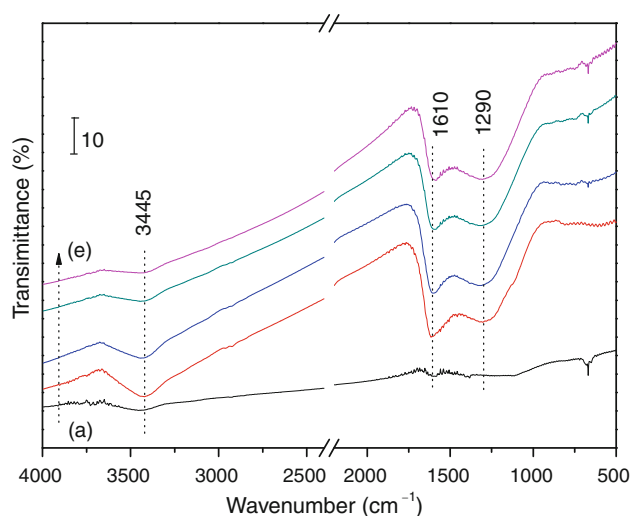


Fig. 5 FT-IR spectra of CN-bulk (a) and CN-MCF-*r* (b–e: *r* = 0.2, 0.4, 0.6, and 0.8) samples

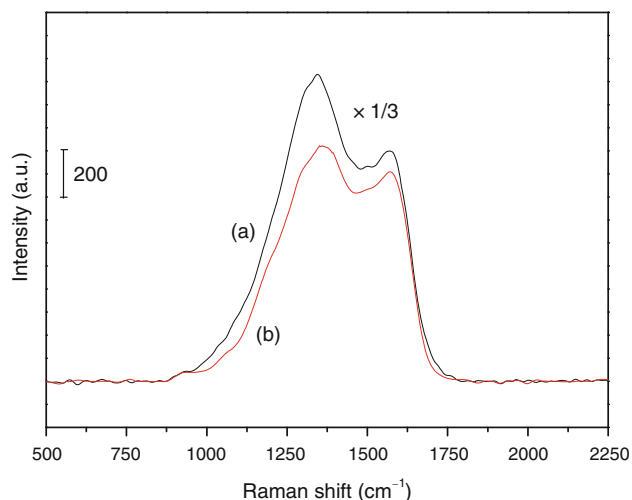


Fig. 6 Raman spectra of CN-bulk (a) and CN-MCF-0.4 (b)

Figure 6 displays the Raman spectra of CN-bulk and CN-MCF-0.4. The spectra exhibit two bands centered at 1,339 and 1,572 cm^{-1} , corresponding to the D (disordered) and G (graphitic) modes of carbon. The results are similar to the Raman modes of previously reported bulk and porous g-CN materials [9, 26]. Compared with CN-MCF-0.4, CN-bulk showed extremely high intensities for the two Raman bands. For the relative I_D/I_G ratio, the value for CN-MCF-0.4 is 1.05, which was much lower than that of CN-bulk (1.42), demonstrating comparatively higher sp^2 -hybridized C species in mesoporous CN-MCF-0.4. This comparison clearly indicates that the introduction of mesoporous structures into CN can improve the amount of graphitic C species.

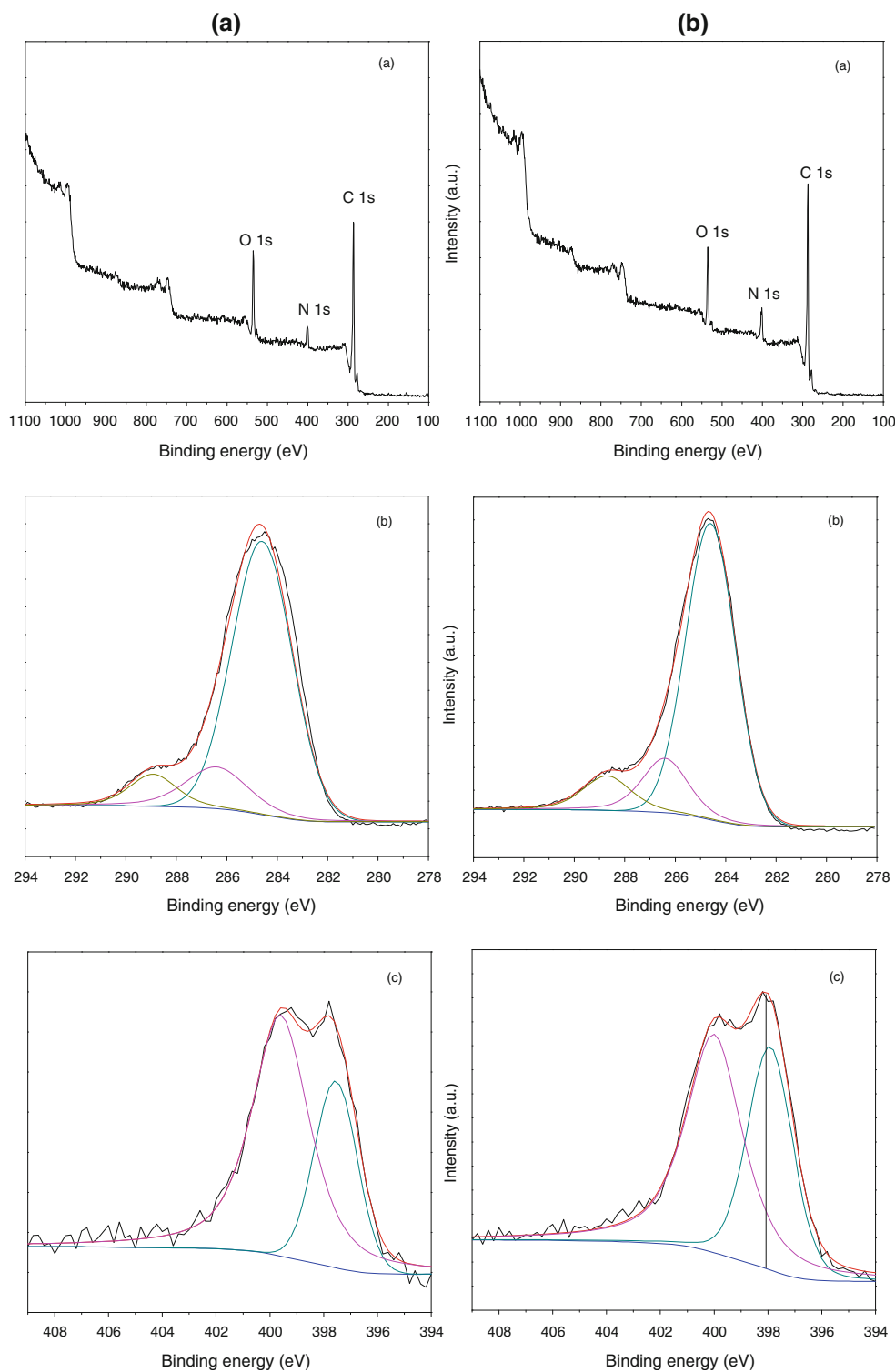
The surface chemical compositions of the materials were further supported by XPS characterization. For

conciseness, only the results of CN-bulk and CN-MCF-0.4 are presented in Fig. 7, and the XP spectra of the other CN-MCF samples are shown in Fig. S1. As illustrated in the survey spectrum (Fig. 7a), the main elements of CN-bulk and CN-MCF-0.4 are C and N, accompanied by a small amount of O species that may come from adsorbed water and partial oxidation of the precursors. It should be also mentioned that the absence of Si element indicates that the silica template is completely removed during the NH_4HF_2 etching process. To probe the detailed chemical states of CN-bulk and CN-MCF-0.4, deconvolution of the C 1s and N 1s peaks was conducted and the results are given in Fig. 7b, c, respectively. For the CN-bulk sample, the C 1s peak (Fig. 7b) can be deconvoluted into three peaks at 289.0, 286.5, and 284.6 eV. The sharp peak at 284.6 eV with high intensity is assigned to pure graphitic sites in the CN matrix, and the peak located at 286.5 eV is attributed to the sp^2 C atoms bonded to N inside the aromatic structures [2, 38]. The highest binding energy at 289.0 eV suggests the presence of sp^2 -hybridized C atoms in the aromatic ring attached to NH_2 groups. In the N 1s spectrum, the peak can also be clearly deconvoluted into two peaks at 399.6 and 397.6 eV. The higher binding energy peak is assigned to the N atoms trigonally bonded to sp^2 or sp^3 C, i.e. tertiary N atoms, while the other is attributed to N atoms sp^2 -bonded to C atoms, e.g. aromatic amines [38]. (Scheme S1). The C 1s and N 1s spectra of CN-MCF-0.4 revealed that its chemical composition is identical to those of CN-bulk. These assignments of XPS data are in line with the values for nonporous [3] and porous g-CN [2] samples reported elsewhere.

3.2 Catalyst Activity

In the present study, owing to their intrinsic N-containing groups, the CN-MCF materials were evaluated as heterogeneous catalysts for Knoevenagel condensation reactions with benzaldehyde and malononitrile as model substrates. The catalytic conversions and selectivities obtained over the CN-MCF materials are over 76 and 92 %, respectively (Table 2), indicating that CN-MCF materials can catalyze the condensation reactions with high efficiency. However, the catalytic activity is closely related to the ratio of EDA/CTC. As the ratio increased, the conversions of benzaldehyde first increased and then decreased slowly, and the best catalytic activity was acquired over CN-MCF-0.4 among the four catalysts (entries 1–4). As mentioned above, Knoevenagel condensation reactions proceed in the presence of the basic catalysts so the catalytic activity is largely dependent on the amount of active sites and textural properties of the catalysts in addition to the reaction conditions. Combining the surface chemical composition (Table 1) and the corresponding catalytic conversions of

Fig. 7 XPS profiles of survey (a), C 1s (b), and N 1s (c) spectra of CN-bulk (a) and CN-MCF-0.4 (b)



the four CN-MCF catalysts, it can be speculated that the highest catalytic activity provided by CN-MCF-0.4 mainly arises from its high N content.

In the XPS characterization, the N spectra (Fig. 7c and Fig. S1) of the CN-MCF materials indicate the presence of

two types of N species, namely N atoms trigonally bonded (399.6 eV) and sp^2 -bonded (397.6 eV) to C atoms. To obtain further insight into the active sites, it is necessary to specify how the two N species affect the catalytic activity. Regarding this, the molar ratios of the trigonally bonded to

sp^2 -bonded N species (n_{NH}/n_{NL} , based on their respectively deconvoluted areas in the XPS spectra) were plotted against with the corresponding conversions in Knoevenagel reactions. As shown in Fig. 8, the values of n_{NH}/n_{NL} correlate well with the catalytic activity, demonstrating that the N atoms trigonally bonded to sp^2 or sp^3 C (i.e. tertiary N atoms) have a positive effect on the catalytic activity.

Table 2 Catalytic activity of CN-MCF samples for Knoevenagel condensation reactions

Entry	Catalyst	Conv. (%)	Sel. (%)	Yield (%)
1 ^a	CN-MCF-0.2	81.4	92.7	75.5
2 ^a	CN-MCF-0.4	84.1	93.6	78.7
3 ^a	CN-MCF-0.6	78.1	92.6	72.3
4 ^a	CN-MCF-0.8	76.5	93.5	71.5
5 ^b	CN-MCF-0.4	96.9	94.7	91.8
6 ^a	CN-bulk-0.4	16.5	92.3	15.3

^a 5 mmol of benzaldehyde and 5 mmol of malononitrile

^b 3 mmol of benzaldehyde and 3 mmol of malononitrile

Figure S2 compares the catalytic conversions and selectivities of CN-MCF-0.4 at different temperatures and reaction time. As the temperature was elevated from 50 to 90 °C, the conversions of reagent increased drastically (Fig. S2a). The selectivities to the products at different temperatures

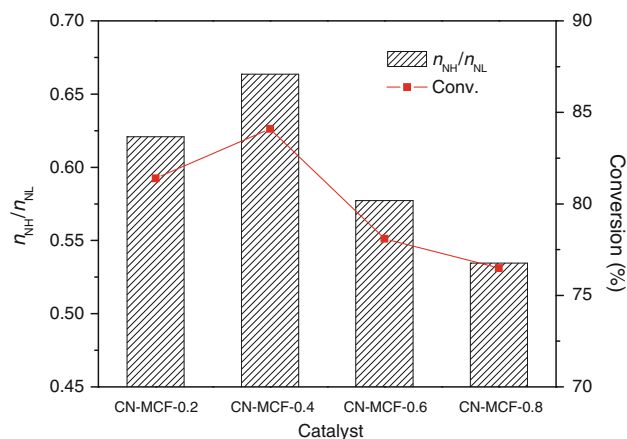
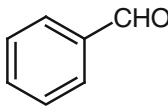
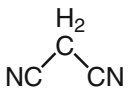
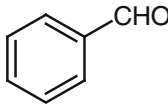
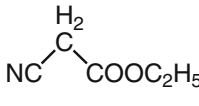
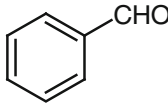
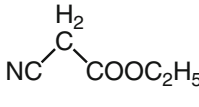
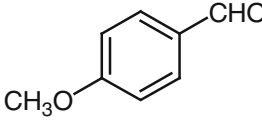
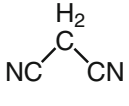
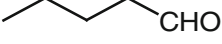
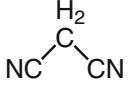
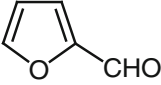
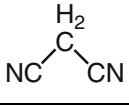


Fig. 8 Correlation between the conversions of the CN-MCF catalysts and the n_{NH}/n_{NL} ratios

Table 3 Various Knoevenagel condensation reactions catalyzed by the CN-MCF-0.4 catalyst

Entry	Aldehyde	Nitrile	Conv. (%)	Sel. (%)
1 ^a			84.1	93.6
2 ^a			3.6	94.3
3 ^b			63.3	95.1
4 ^a			69.7	94.4
5 ^a			71.0	93.7
6 ^a			84.7	93.2

Reaction condition: 5 mmol of aldehyde, 5 mmol of methylene group-containing nitrile, 0.3 mL of *n*-decane as internal standard, 100 mg of catalyst. Catalytic tests were performed at 90 °C and the catalytic results were collected after 4 h

^a 5 mL of CH_3CN as solvent

^b 5 mL of *n*-butanol as solvent

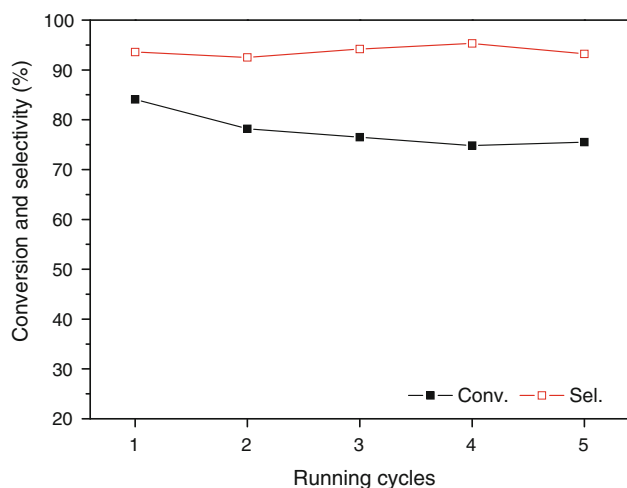


Fig. 9 Evolution of catalytic performance of Knoevenagel condensation reactions during five tests

were all higher than 88 %, and the byproduct was mainly benzoic acid that originated from the auto-oxidation of benzaldehyde under ambient atmospheric conditions [14]. The conversion and selectivity as a function of reaction time is given in Fig. S2b. At 0.5 h, the reaction proceeded with a moderate conversion of 48 %. As the reaction was prolonged over 4 h, maximum conversion was reached. Regarding the effect of reaction conditions on their corresponding catalytic performance, a temperature of 90 °C and reaction time of 4 h were chosen as suitable reaction conditions for the further catalytic investigation.

Besides the reaction temperature and time, the recycling capability is also of importance for the evaluation of a heterogeneous catalyst. Consequently, a series of experiments were performed to test the reusability of the catalyst and reproducibility of catalytic performance. As shown in Fig. 9, the selectivities obtained in these cycles are all above 92 %. For the conversion, a decrease of ca. 6 % was observed for the first recycling step, and this could be due to the partial leaching of N-containing fragments located at the edges of the graphitic layers [30]. In spite of the initial decline, the subsequent tests showed stable catalytic activity, suggesting that the CN-MCF material can be used as a stable heterogeneous catalyst for Knoevenagel condensation reactions.

To investigate the catalytic versatility of CN-MCF, a series of Knoevenagel condensation reactions between various aldehydes and methylene-group-containing nitriles (Table 3) were conducted in the presence of CN-MCF-0.4. In addition to aromatic aldehydes (entries 1 and 4), aliphatic aldehydes such as pentanal and furfural aldehyde (entries 5 and 6) could also undergo condensation reactions with malononitrile and offer efficient conversions. Furthermore, different active methylene compounds were

compared under the same catalytic conditions. With ethyl cyanoacetate (ECA), the reaction gave a low catalytic activity (entry 2), probably because the electron withdrawing ability of the substituent $-\text{COOR}$ in ECA is relatively weaker compared to that of $-\text{C}\equiv\text{N}$. Nevertheless, a moderate yield was obtained if the reaction was performed in a protic solvent (entry 3).

4 Conclusion

In summary, a series of 3D mesostructured g-CN materials were synthesized using MCF as a template, and CTC and EDA as precursors. By altering the EDA/CTC ratio between 0.4 and 0.8, CN-MCF was obtained with tunable surface areas and pore volumes and a uniform pore size of ca. 5.2 nm. Among the various CN-MCF samples prepared with different EDA/CTC ratios, CN-MCF-0.4 demonstrated the highest catalytic activity for Knoevenagel condensation reactions, affording a high conversion of 84.1 %. Furthermore, the catalytic performances of CN-MCF-0.4 in the recycling tests and with various substrates show its efficiency and versatility towards a series of Knoevenagel condensation reactions.

Acknowledgments This work was supported by National Natural Science Foundation of China (21203014), CNPC Innovation Foundation (2011D-5006-0508), Open Foundation of Shanghai Key Laboratory of Molecular Catalysts and Innovative Materials attached to Fudan University (2011MCIMKF01), Open Foundation of Jiangsu Key Laboratory of Fine Petrochemical Engineering attached to Changzhou University (KF1201), and the project funded by the Priority Academic Program Development of Jiangsu Higher Education Institutions. Jie Xu also thanks Mrs. Li-Juan Zhang and Prof. Wei-Lin Dai, Fudan University for their kind help with SAXS and XPS characterization.

References

- Kroke E, Schwarz M (2004) *Coord Chem Rev* 248:493–532
- Vinu A (2008) *Adv Funct Mater* 18:816–827
- Qiu Y, Gao L (2003) *Chem Commun* 18:2378–2379
- Xia X, Zhou C, Tong D, Liu M, Zhang D, Fang M, Yu W (2010) *Mater Lett* 64:2620–2623
- Lee EZ, Jun Y-S, Hong WH, Thomas A, Jin MM (2010) *Angew Chem Int Ed Engl* 49:9706–9710
- Wang Y, Wang X, Antonietti M (2012) *Angew Chem Int Ed Engl* 51:68–89
- Goettmann F, Fischer A, Antonietti M, Thomas A (2006) *Angew Chem Int Ed Engl* 45:4467–4471
- Park SS, Chu S-W, Xue C, Zhao D, Ha C-S (2011) *J Mater Chem* 21:10801–10807
- Li Q, Yang J, Feng D, Wu Z, Wu Q, Park SS, Ha C-S, Zhao D (2010) *Nano Res* 3:632–642
- Zhang Y, Mori T, Ye J, Antonietti M (2010) *J Am Chem Soc* 132:6294–6295
- Kim M, Hwang S, Yu J-S (2007) *J Mater Chem* 17:1656–1659

12. Wang X, Maeda K, Thomas A, Takanabe K (2009) *Nat Mater* 8:76–80
13. Maeda K, Wang X, Nishihara Y, Lu D, Antonietti M, Domen K (2009) *J Phys Chem C* 113:4940–4947
14. Su F, Antonietti M, Wang X (2012) *Catal Sci Tech* 2:1005–1009
15. Goettmann F, Fischer A, Antonietti M, Thomas A (2006) *Chem Commun* 119:4530–4532
16. Goettmann F, Fischer A, Antonietti M, Thomas A (2007) *New J Chem* 31:1455–1460
17. Goettmann F, Thomas A, Antonietti M (2007) *Angew Chem Int Ed Engl* 46:2717–2720
18. Jin X, Balasubramanian VV, Selvan ST, Sawant DP, Chari MA, Lu GQ, Vinu A (2009) *Angew Chem Int Ed Engl* 48:7884–7887
19. Groenewolt M, Antonietti M (2005) *Adv Mater* 17:1789–1792
20. Wang Y, Wang X, Antonietti M, Zhang Y (2010) *ChemSusChem* 3:435–439
21. Ansari MB, Min B-H, Mo Y-H, Park S-E (2011) *Green Chem* 13:1416–1421
22. Ansari MB, Jin H, Parvin MN, Park S-E (2012) *Catal Today* 185:211–216
23. Wu Z, Webley PA, Zhao D (2012) *J Mater Chem* 22:11379–11389
24. Zhang Y, Mori T, Ye J (2012) *Sci Adv Mater* 4:282–291
25. Vinu A, Ariga K, Mori T, Nakanishi T, Hishita S, Golberg D, Bando Y (2005) *Adv Mater* 17:1648–1652
26. Liu L, Ma D, Zheng H, Li X, Cheng M, Bao X (2008) *Micropor Mesopor Mater* 110:216–222
27. Vinu A, Srinivasu P, Sawant DP, Mori T, Ariga K, Chang J-S, Jung S-H, Balasubramanian VV, Hwang YK (2007) *Chem Mater* 19:4367–4372
28. Saravanamurugan S, Palanichamy M, Hartmann M, Murugesan V (2006) *Appl Catal A* 298:8–15
29. Zhang X, Man Lai ES, Martin-Aranda R, Yeung KL (2004) *Appl Catal A-Gen* 261:109–118
30. Freire RM, Morais Batista AH, Souza Filho AG, Filho JM, Saraiva GD, Oliveira AC (2009) *Catal Lett* 131:135–145
31. Kan-Nari N, Okamura S, Fujita S-I, Ozaki J-I, Arai M (2010) *Adv Synth Catal* 352:1476–1484
32. Schmidt-Winkel P, Lukens WW, Zhao D, Yang P, Stucky G, Chmelka B (1999) *J Am Chem Soc* 121:254–255
33. Schmidt-Winkel P, Lukens WW, Yang P, Margolese DI, Lettow JS, Ying JY, Stucky GD (2000) *Chem Mater* 12:686–696
34. Mane GP, Talapaneni SN, Anand C, Varghese S, Iwai H, Ji Q, Ariga K, Mori T, Vinu A (2012) *Adv Funct Mater* 22:3596–3604
35. Liu Y, Feng W, Li T, He H, Dai W, Huang W, Cao Y, Fan K (2006) *J Catal* 239:125–136
36. Lettow JS, Han YJ, Schmidt-Winkel P, Yang P, Zhao D, Stucky GD, Ying JY (2000) *Langmuir* 16:8291–8295
37. Talapaneni SN, Anandan S, Mane GP, Anand C, Dhawale DS, Varghese S, Mano A, Mori T, Vinu A (2012) *J Mater Chem* 22:9831–9840
38. Srinivasu P, Vinu A, Hishita S, Sasaki T, Ariga K, Mori T (2008) *Micropor Mesopor Mater* 108:340–344